The International Journal of Advanced Manufacturing Technology (2018) 98:487–504
https://doi.org/10.1007/s00170-018-2279-0

ORIGINAL ARTICLE

A moving knot sequence-based feedrate scheduling method of parametric interpolator for CNC machining with contour error and drive constraints

Mansen Chen[1] · Yuwen Sun[1]

Received: 31 December 2017 / Accepted: 4 June 2018 / Published online: 12 June 2018

Abstract
The feedrate scheduling of parametric interpolator is one of the most important factors for a high-performance CNC machining, since it directly concerns the machining efficiency, machining accuracy, and cutting stability. In this paper, an adaptive feedrate scheduling method with limited contour error and axis jerks is proposed for free-form contour machining based on a strategy of moving knot sequence. The analytical relations between dynamic contour error and feedrate are first derived explicitly, and then the formula of maximum feedrate limit under confined contour error and axis jerks is yielded using a numerical decoupling scheme. Consequently, the maximum feedrate limit satisfying the above constraints is obtained for each predefined parametric segment of the tool path. Further, a bidirectional scanning algorithm is employed to globally adjust the local minimum feedrate values of all feedrate segments. On the basis of feedrate segments with local minimum value and maximum recommendation value, an exact knot sequence configuration method for the B-spline curve, which is used to express the initial feedrate profile, is proposed. Finally, a simple feedrate relaxation algorithm is performed to generate the final feedrate profile with entirely limited contour and axis jerks by utilizing a strategy of moving knot sequence. The proposed feedrate scheduling method is validated by several typical experimental tests, and the results demonstrate the effectiveness and reliability of the proposed method.

Keywords Parametric interpolator · Feedrate scheduling · Contour error · Axis jerks

1 Introduction

With the growing demand for higher productivity and better machining accuracy, computer numerical control (CNC) machine tools have been widely applied in modern automated manufacturing industry. In conventional CNC systems, only the function of linear/circular interpolation is provided. Therefore, most of the complex tool paths designed in computer-aided manufacturing (CAM) software have to be segmented into a huge number of short linear segments or circular arcs in the post-processors. However, the large size of the NC data will inevitably increase the CNC data transfer burden, and the curvature discontinuities of consecutive segments at the junction might lead to abrupt change of tangential acceleration or jerk, thus causing unwanted vibrations and deteriorating the contouring performance [1]. In contrast, parametric interpolation due to its advantages of reduced size of NC codes and improved path smoothness is gaining increasing attention from the scholars. As a basic input of parametric interpolator, the feedrate profile scheduled by the CNC system plays a fundamental role in achieving high-efficiency machining. However, limited to the bandwidth of servo drives, the programmed feedrate in a regular NC machining is often kept at a conservative level to prevent mechanical shock to the cutter and machine. As a consequence, a longer machining time is inevitable. To handle this issue, significant effort has been devoted to the feedrate scheduling methods under the various kinematical constraints [2–34]. On the other hand, to guarantee a required machining accuracy of the final product, the importance of constraining contour error has been also well recognized in recent years. Therefore, how to schedule a smooth feed profile, which is capable of simultaneously considering the kinematical performance of machine tool and

✉ Yuwen Sun
xiands@dlut.edu.cn

[1] Key Laboratory for Precision and Non-Traditional Machining Technology of the Ministry of Education, Dalian University of Technology, Dalian 116024, China

contouring accuracy requirement, is quite meaningful for the development of high-performance CNC machine.

To maintain a stable cutting process, some constant feedrate interpolation methods are often adopted in the earlier works [35, 36], but the geometrical constraint is not considered in their works. Afterwards, Yeh and Hsu [2] incorporate the constraint of chord error into feedrate scheduling model to enhance the machining accuracy based on the geometrical properties of path curve. And, for preventing abrupt change of cutting tool at the sharp corners or sensitive regions with tight curvature of path curve, Cheng and Tsai [3] developed a variable feedrate scheduling method for parametric interpolator with consideration of the tangential acceleration limitation. Yong and Narayanaswami [4] also proposed an adaptive feedrate scheduling method under the combined constraints of chord error and acceleration. Meanwhile, some jerk-limited feedrate scheduling methods, such as the look-ahead strategy [5–13], sine-curve [14–17], s-curve [18–22], and polynomial function [23–25], are also subsequently proposed with a smoother kinematic characteristic of path curve. Need to note that the abovementioned algorithms are mainly focused on enhancing the tangential kinematical performance without considering the drivers' ability of machine tool. As a result, the feedrate command has to be set strictly in order to avoid the violation of physical limits of drivers, especially for the case of five-axis machining. To handle this issue, the drive constraints in terms of the velocity, acceleration, and jerk of each axis are also needed to be confined within a specified range during the feedrate scheduling. Until now, such issue has been stressed by using the bidirectional scanning [26, 27], greedy algorithms [28], and linear programming algorithms [29–31]. In addition, Beudaert et al. [32] also introduced an iterative algorithm based on a dichotomy and look-ahead strategy to obtain an optimized feedrate profile with confined axis jerk constraints. Sencer et al. [33] predefines the feedrate profile as a cubic B-spline curve, thus the constraint-limited feedrate scheduling is reduced to a constrained optimization problem, which can be solved by using the sequential quadratic programming methods. Moreover, Mansour and Seethaler [34] also proposed a real-time feedrate optimization algorithm with confined axial acceleration based on their induced control architecture that integrates both modeled and measured process data.

For a higher precision machining, calculation of contour error is an essential step toward achieving the feedrate scheduling with a confined contour error. However, it is difficult to obtain an analytical solution of contour error for a free from curve in comparison to the linear or circular path. Hence, many scholars often attempt to calculate an approximate contour error instead, rather than to compute the actual one [37–45]. For example, Chuang and Liu [37] developed a linear approximation approach to estimate the contour error for arbitrary path curve. Yeh and Hsu [38, 39] approximated the contour error by projecting the tracking error vectors on the normal direction of the trajectory at the reference points. And, Chen et al. [40] introduced a novel linear approximation model, in which they show that the contour error can be well approximated by the distance from the actual tool position to the tangential circle on the reference point. Moreover, some other error estimation methods with real-time performance are also consecutively proposed by Zhu et al. [43], Pi et al. [44], and Yang et al. [45].

On this basis, various contour error control methods are simultaneously developed. However, most of the current studies are focused on design of servo controller, such as the cross-coupled control [46, 47], sliding mode control [48], iterative learning control [49], model predictive control [50, 51], and adaptive control [52]. By contrast, the feedrate scheduling methods with consideration of contour error are very limited [53–58]. For example, Lin et al. [55] introduced a real-time parametric interpolator to obtain a smooth and contour error limited feedrate profile based on a look-ahead scheme and a servo dynamics model. And, for the case of discrete line paths, Dong et al. [56] presented a contour error-limited feedrate planning methods by simplifying the dynamic of feed drives as a one-order inertial system. In addition, Dong et al. [57] incorporated the contour error and axis acceleration constraint into the two-pass iterative algorithms to achieve a satisfactory contouring performance. And Jia et al. [58] also proposed a feedrate scheduling method for NURBS interpolator, in which a constant speed is employed at sensitive regions of contour error to ensure the cutting stability. Based on the different constraints limited in the feedrate scheduling, these representative studies are summarized in Table 1.

From Table 1, it can be seen that the feedrate scheduling methods with integrated constraints of contour error and axis jerks are rarely considered in existing studies. And the aim of this paper is to present a novel feedrate scheduling method to simultaneously constrain the contour error and axis jerk without excessive computation complexity. The main contribution of this paper is to yield an explicit relationship between the dynamic contour error and feedrate; thus, the contour error constraint for a CNC machining is reduced to a kinematic constraint, which sets up a bridge between the contour error control and feedrate scheduling. On this basis, in order to achieve a smooth axial dynamic performance, a feedrate relaxation algorithm based on a decoupling scheme and a moving knot sequence strategy is subsequently introduced with confined contour error and axis jerk. Besides, to avoid the high-frequency vibration induced by the discontinuous tangential acceleration, the smoothness of feedrate is ensured by using a B-spline curve with an accurate configuration of knot sequence. The remainder of this paper is organized as follows: Section 2 gives a relation model between contour error and feedrate according to a general second order servo system. Section 3 introduces the related contour error and

Table 1 Comparison of feedrate scheduling methods

Papers	Limited constraints				
	Tangential acc	Tangential jerk	Axial acc	Axial jerk	Contour error
[3, 4]	Yes	No	No	No	No
[5–25]	Yes	Yes	No	No	No
[29, 34]	No	No	Yes	No	No
[26–28, 30–33]	No	No	Yes	Yes	No
[55, 56, 58]	Yes	Yes	No	No	Yes
[53, 54, 57]	No	No	Yes	No	Yes

drive constraints and their satisfaction conditions. Detailed implementations of the proposed feedrate scheduling method are described in Section 4. Experimental results and discussions are given in Section 5 and Section 6 concludes the paper.

2 Contour error model

Limited by bandwidth of servo systems, contour errors are inevitably generated if one of the servo axes is not able to follow the reference command accurately. In order to estimate contour error that arises from the servo systems, a commonly used proportional controller, which has the advantages of simple structure, easy control, and reliability, is employed in the position-feedback loops as shown in Fig. 1. Then, the corresponding closed-loop transfer function can be derived as

$$G(s) = \frac{y(s)}{r(s)} = \frac{k_p k_t k_a}{Js^2 + Bs + k_p k_t k_a} \tag{1}$$

where $r(s)$ represents the reference input, $y(s)$ represents the actual output, k_p is the proportional gain, k_t is the motor constant, k_a is ball-screw constant, J is the inertia, and B is the viscous friction coefficient.

Denoting $w_n = \sqrt{k_p k_t k_a / J}$, $\xi = B/2J\sqrt{k_p k_t k_a}$, the transfer function in Eq. (1) can be further expressed as the following second-order system

$$G(s) = \frac{y(s)}{r(s)} = \frac{w_n^2}{s^2 + 2\xi w_n s + w_n^2} \tag{2}$$

where w_n represents the natural frequency and ξ is the damping ratio. For a given third or much higher order systems,

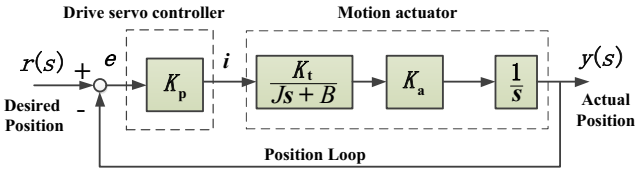

Fig. 1 Block diagram for individual drive axis with P-controller

it is also permissible to simplify them as the above uniform second-order systems according to the method of predominate poles. Accordingly, the error transfer function of the close loop system can be obtained as follows

$$G_e(s) = \frac{e(s)}{r(s)} = \frac{s^2 + 2\xi w_n s}{s^2 + 2\xi w_n s + w_n^2} \tag{3}$$

Given a ramp position input signal $r(s) = V_i/s^2$, where V_i $(i = x, y)$ represents the desired axial velocity, the tracking error can be expressed as

$$E(s) = \frac{V_i\, s^2 + 2V_i\, \xi w_n s}{s^4 + 2\xi w_n s^3 + w_n^2 s^2} \tag{4}$$

Utilizing the final-value theory, the steady-state tracking error is then derived as

$$e(\infty) = \lim_{s\to 0} sE(s) = \frac{2V_i\, \xi}{w_n} \tag{5}$$

By denoting $K_{ei} = \frac{w_n}{2\xi}$, Eq. (5) is further rewritten as

$$e(\infty) = \lim_{s\to 0} sE(s) = \frac{V_i}{K_{ei}} \tag{6}$$

For a specified servo feed system, w_n and ξ are normally constant coefficients. Therefore, according to Eq. (6), it can be inferred that the steady-state tracking error is only dependent on the axial velocity V_i, which actually provides a premise to find an analytical relationship between the feedrate f and contour error. Consequently, a model for calculating the maximum allowable feedrate constrained by contour error can be built.

As illustrated in Fig. 2, for an arbitrary parametric tool path $\boldsymbol{P}(u)$, assuming A is the actual interpolation point, N is the nearest point to A, and D is the reference interpolation point, then the tracking error and contour error can be denoted as the distance $\overline{AD}$ and $\overline{AN}$, respectively. For simplifying the computation complexity of contour error for a free-form path contour, as shown in Fig. 2, the osculating circle is a better approximation to the curve segment of the tool path at the

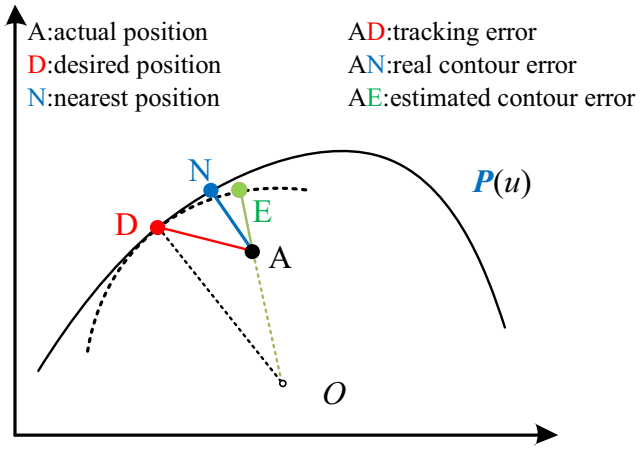

Fig. 2 Contour error for a free-form curve

reference interpolation point. Accordingly, the contour error $\overline{AN}$ can be estimated by the radial distance $\overline{AE}$.

Assuming the radius of the osculating circle at the given reference interpolation point of the tool path $\boldsymbol{P}(u)$ is r, as shown in Fig. 3, the corresponding circular contour can be expressed as

$$x_d^2 + y_d^2 - r^2 = 0 \tag{7}$$

In Cartesian coordinates, let $x_a = x_d + E_x$ and $y_a = y_d + E_y$, then one can have

$$(x_d + E_x)^2 + (y_d + E_y)^2 = (r + \varepsilon)^2 \tag{8}$$

where ε represents the contour error, E_x and E_y are the tracking errors of X and Y axes, respectively.

By denoting $E_x = V_x/K_{ex}$ and $E_y = V_y/K_{ey}$ according to Eq. (6), Eq. (8) becomes

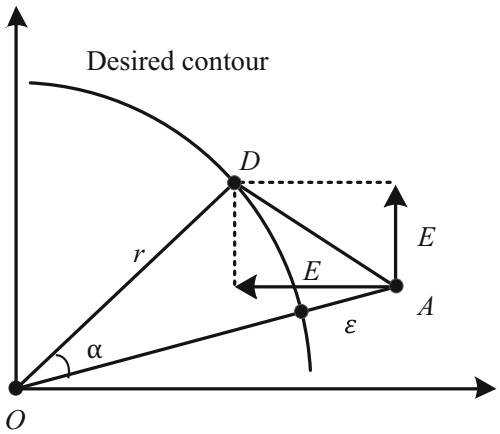

Fig. 3 Contour error for an osculating circle

$$x_d^2 + y_d^2 + \left(\frac{V_x}{K_{ex}}\right)^2 + \left(\frac{V_y}{K_{ey}}\right)^2 + \frac{2x_d V_x}{K_{ex}} + \frac{2y_d V_x}{K_{ey}} = r^2 + \varepsilon^2 + 2r\varepsilon \tag{9}$$

Then, taking the derivate of Eq. (7) with respect to time, one can have

$$x_d V_x + y_d V_y = 0 \tag{10}$$

For a matched axial dynamics system with $K_{ex} = K_{ey} = K_e$, one can substitute Eqs. (7) and (10) into Eq. (9) and obtain

$$V_x^2 + V_y^2 = K_e^2(\varepsilon^2 + 2r\varepsilon) \tag{11}$$

Since $V_x^2 + V_y^2 = f^2$, the steady-state contour error can be further derived as

$$\varepsilon = -r + \sqrt{r^2 + \frac{f^2}{K_e^2}} \tag{12}$$

Thus, for a given parametric tool path $\boldsymbol{P}(u)$, the corresponding contour error can be calculated by

$$\varepsilon = -\frac{1}{\rho(u)} + \sqrt{\frac{1}{\rho^2(u)} + \frac{f^2}{K_e^2}} \tag{13}$$

where $\rho(u)$ represents the curvature of the tool path $\boldsymbol{P}(u)$ and has the following expression

$$\rho(u) = \frac{\|\dot{\boldsymbol{P}} \times \ddot{\boldsymbol{P}}\|}{\|\dot{\boldsymbol{P}}\|^3} \tag{14}$$

3 Feedrate limit with multi-constraints

3.1 Contour error constraint

According to Eq. (13), in order to limit the contour error within a prescribed range, the following equation should be satisfied

$$\varepsilon = -\frac{1}{\rho(u)} + \sqrt{\frac{1}{\rho^2(u)} + \frac{f^2(u)}{K_e^2}} \le \varepsilon_{max} \tag{15}$$

where $f(u)$ is the velocity along the tool path. Given a maximum allowable contour error ε_{max}, the feasible feedrate with constraint of contour error can be expressed as

$$f(u) \le K_e \sqrt{\varepsilon_{max}^2 + \frac{2\varepsilon_{max}}{\rho(u)}} \tag{16}$$

3.2 Drive constraints

Along a given parametric tool path $\boldsymbol{P}(u)$, assuming the nominal feedrate is specified as $f(u)$, then the related velocity, acceleration, and jerk for each individual drive can be calculated by

$$\begin{cases} \boldsymbol{V}_\tau(u) = \dot{\boldsymbol{P}}_\tau(u)\dfrac{du}{ds}f(u) \\ \boldsymbol{A}_\tau(u) = \left(\ddot{\boldsymbol{P}}_\tau(u)\left(\dfrac{du}{ds}\right)^2 + \dot{\boldsymbol{P}}_\tau(u)\dfrac{d^2u}{ds^2}\right)f^2(u) + \dot{\boldsymbol{P}}_\tau(u)\dfrac{du}{ds}A_c(t) \\ \boldsymbol{J}_\tau(u) = \left(\dddot{\boldsymbol{P}}_\tau(u)\left(\dfrac{du}{ds}\right)^3 + 3\ddot{\boldsymbol{P}}_\tau(u)\dfrac{du}{ds}\dfrac{d^2u}{ds^2} + \dot{\boldsymbol{P}}_\tau(u)\dfrac{d^3u}{ds^3}\right)f^3(u) \\ \quad +3\left(\ddot{\boldsymbol{P}}_\tau(u)\left(\dfrac{du}{ds}\right)^2 + \dot{\boldsymbol{P}}_\tau(u)\dfrac{d^2u}{ds^2}\right)f(u)A_c(t) + \dot{\boldsymbol{P}}_\tau(u)\dfrac{du}{ds}J_c(t) \end{cases} \tag{17}$$

where $\boldsymbol{P}_\tau(u)(\tau = x, y)$ indicates the coordinate component of the tool path curve $\boldsymbol{P}(u)$, and s represents the arc length parameter. Additionally, the derivatives of path parameter u with respect to arc length parameter s can be derived as follows

$$\begin{cases} \dfrac{du}{ds} = \dfrac{1}{\|P_u(u)\|} \\ \dfrac{d^2u}{ds^2} = -\dfrac{P_u(u)\cdot P_{uu}(u)}{\|P_u(u)\|^4} \\ \dfrac{d^3u}{ds^3} = \dfrac{3P_u(u)\cdot P_{uu}(u)}{\|P_u(u)\|^6} - \dfrac{\|P_{uu}(u)\|^2 + P_u(u)\cdot P_{uuu}(u)}{\|P_u(u)\|^5} \\ \quad -\dfrac{(P_u(u)\cdot P_{uu}(u))^2}{\|P_u(u)\|^7} \end{cases} \tag{18}$$

where $A_c(t)$ and $J_c(t)$ represent the tangential acceleration and tangential jerk of feedrate profile, and they are expressed as

$$\begin{cases} A_c(t) = \dfrac{df}{dt} = f_u f \dfrac{du}{ds} \\ J_c(t) = \dfrac{dA_c}{dt} = \left(f_{uu}f^2 + f_u^2 f\right)\left(\dfrac{du}{ds}\right)^2 + \dfrac{d^2u}{d^2s}f_u f^2 \end{cases} \tag{19}$$

To avoid violating the physical saturation limits of servo drives, the kinematical constraints of each axis in terms of velocity, acceleration, and jerk should be confined within a prescribed range, that is, the following equation should be satisfied

$$-\begin{bmatrix} V_{\tau,max} \\ A_{\tau,max} \\ J_{\tau,max} \end{bmatrix} < \begin{bmatrix} \boldsymbol{V}_\tau(u) \\ \boldsymbol{A}_\tau(u) \\ \boldsymbol{J}_\tau(u) \end{bmatrix} < \begin{bmatrix} V_{\tau,max} \\ A_{\tau,max} \\ J_{\tau,max} \end{bmatrix} \ (\tau = x, y) \tag{20}$$

which is not only beneficial to preventing excessive shocks and vibrations to the machine tool, but also favorable to fully exploiting the capabilities of feed system.

3.3 Determination of feedrate limit under multi-constraints

From Eq. (17), it reveals that the axial dynamics is combinedly affected by both the kinematic performance of feed movement and the geometric performance of path curve, including the feedrate $f(u)$ itself, the tangential acceleration A_c, and tangential jerk J_c of feedrate profile $f(u)$, as well as the derivatives $\dot{\boldsymbol{P}}_\tau(u)$ $\ddot{\boldsymbol{P}}_\tau(u)$, and $\boldsymbol{P}_\tau(u)$ of the path curve $\boldsymbol{P}(u)$. In other words, it is very difficult to analytically determine a suitable feedrate value for each independent interpolation point under axis jerk constraints. Exceptionally, if the feedrate is kept constant at some fixed parameter interval, the maximum feedrate allowed by the axis jerks can be obtained immediately since $A_c(t) = 0$ and $J_c(t) = 0$. The similar case occurs at the extremal position of the feedrate curve, in which the calculation of axis accelerations $\boldsymbol{A}_\tau(u)$ is position-dependent since $A_c(t) = 0$. Further, if a microsegment of constant feedrate is specified around the extremal position where the approaching feedrate is decelerating and then increasing, the axis jerks $\boldsymbol{J}_\tau(u)$ will be also position-dependent. This hints us that exact feedrate limits

constrained by axis jerks can be obtained at the positions of constant speed or corner point of feedrate profile.

Thus, at these positions where $A_c(t)=0$ and $J_c(t)=0$, it becomes possible to calculate axial jerks using a decoupling scheme. Accordingly, Eq. (17) is simultaneously rewritten as

$$\begin{cases} \boldsymbol{V}_\tau(u) = \boldsymbol{C}_\tau^v f(u) \\ \boldsymbol{A}_\tau(u) = \boldsymbol{C}_\tau^a f^2(u) \\ \boldsymbol{J}_\tau(u) = \boldsymbol{C}_\tau^j f^3(u) \end{cases} \tag{21}$$

where

$$\begin{cases} \boldsymbol{C}_\tau^v = \dot{\boldsymbol{P}}_\tau(u)\dfrac{du}{ds} \\ \boldsymbol{C}_\tau^a = \ddot{\boldsymbol{P}}_\tau(u)\left(\dfrac{du}{ds}\right)^2 + \dot{\boldsymbol{P}}_\tau(u)\dfrac{d^2u}{ds^2} \\ \boldsymbol{C}_\tau^j = \boldsymbol{P}_\tau(u)\left(\dfrac{du}{ds}\right)^3 + 3\ddot{\boldsymbol{P}}_\tau(u)\dfrac{du}{ds}\dfrac{d^2u}{ds^2} + \dot{\boldsymbol{P}}_\tau(u)\dfrac{d^3u}{ds^3} \end{cases} \tag{22}$$

For a fixed parameter position u of path curve $\boldsymbol{P}(u)$, the coefficients $\boldsymbol{C}_\tau^v$, $\boldsymbol{C}_\tau^a$, and $\boldsymbol{C}_\tau^j$ are constant, since their values are only dependent on the geometric characteristics of the known tool path $\boldsymbol{P}(u)$. Therefore, an exact solution of feedrate limit with contour error and drive constraints can be given

$$f(u) = \min_{\tau=x,y}\left(f_{max}, K_e\sqrt{\varepsilon_{max}^2 + \frac{2\varepsilon_{max}}{\rho(u)}}, \frac{V_{\tau,max}}{\left|\boldsymbol{C}_\tau^v\right|}, \frac{A_{\tau,max}}{\left|\boldsymbol{C}_\tau^a\right|}, \frac{J_{\tau,max}}{\left|\boldsymbol{C}_\tau^j\right|}\right) \tag{23}$$

where f_{max} represents the maximum programmed feedrate. Utilizing these exact feature values at constant segments and extremal positions of feedrate profile, the issue of feedrate scheduling with above constraints can be reduced from global optimization to the local curve construction based on exact extreme points.

4 Feedrate scheduling algorithm

For a given NURBS tool path $\boldsymbol{P}(u)$, an efficient feedrate scheduling algorithm with confined contour error and axis jerks is developed as a preprocessor, which is able to reduce the computational burden in real-time NURBS interpolator. Figure 4 shows the flowchart of the proposed feedrate scheduling method. The whole scheduling process is divided into three modules, namely, feedrate limit calculation module, local minimum feedrate correction module, and feedrate relaxation module. In the feedrate limit calculation module, the feedrate limit is obtained for each subdomain of tool path $\boldsymbol{P}(u)$ using formula (23), and then the adjacent subdomains which have slightly different feedrates are merged together. Afterwards, in the second module, local minimum feedrates among all feedrate segments are detected, and then a set of updated local minimum feedrates without violating the constraints is determined by using a bidirectional scanning strategy. In the third module, based on the featured feedrates with local minimum values or maximum ones, a configuration method of exact knot sequence of B-spline curve used to express the initial feedrate profile is proposed, and a moving knot sequence-based feedrate relaxation algorithm is employed to generate the final feedrate profile with confined contour error and drive constraints.

4.1 Feedrate limit calculation module

In order to determine the exact feedrate limits and their corresponding parametric locations along the given path curve, a numerical discretization is conducted on the parameter domain of the entire tool path $\boldsymbol{P}(u)$ with a user-defined parameter interval Δu. Without losing generality, assuming that the parameter range of the tool path is defined as [0,1], then the parameter segment for each interval Δu is denoted as

$$\begin{cases} \left[\overline{u}_i\right]_{i=1}^{M} = \left[(i-1)\Delta u, i\Delta u\right]_{i=1}^{M} = [0,1] \\ \overline{u}_i^- = (i-1)\Delta u \\ \overline{u}_i^+ = i\Delta u \end{cases} \tag{24}$$

where M represents the discrete number, $\overline{u}_i^-$ represents the left boundary of the segment $[\overline{u}_i]$, and $\overline{u}_i^+$ represents the right boundary.

For achieving the maximum reachable feedrate $f([\overline{u}_i])$ for each parameter segment, a small number of points $u_{i,j}(j=1, 2, \ldots N)$ also needs to be sampled at $[\overline{u}_i]$. Then, one can get the maximum feedrate $f(u_{i,j})$ of each sampling position $u_{i,j}$ by utilizing Eq. (23). Subsequently, the maximum feedrate limit $f([\overline{u}_i])$ for each segment can be further derived through Eq. (25)

$$f\left(\left[\overline{u}_i\right]\right) = \min\left\{f\left(u_{i,j}\right)\right\}(j=1,2,\ldots N) \tag{25}$$

Then, as illustrated in Fig. 5(a), the maximum reachable feedrate sequence $[f_i]_{i=1}^{M}$ is finally constructed. Further, if the feedrate values of the adjacent feedrate segments fluctuate within a small range, a merging operation is carried out to maintain a stable cutting movement without excessive feedrate fluctuations. Just as shown in Fig. 5(b), $[\overline{u}_i]_{i=3}^{4}$ are merged together as $[\overline{u}_r]_{r=3}$, and $[\overline{u}_i]_{i=7}^{12}$ are merged as $[\overline{u}_r]_{r=6}$. Besides, the merged feedrate value is simultaneously updated as $f([\overline{u}_r]) = \min(f([\overline{u}_i]))$. Thus, the local minimum and maximum feedrates and their associated parameter regions can be determined rapidly along the entire tool path.

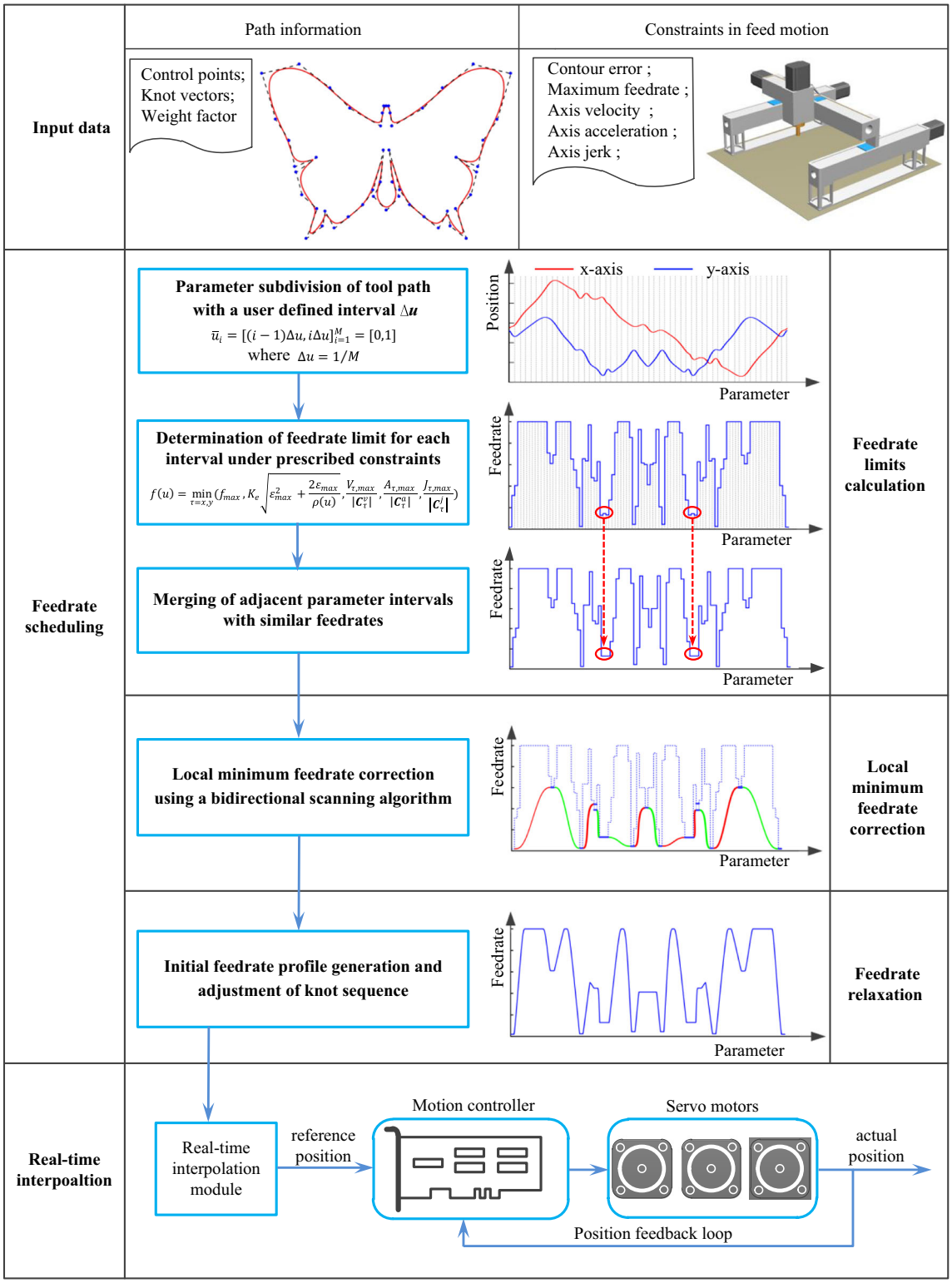

Fig. 4 The flowchart of the proposed feedrate scheduling method

4.2 Local minimum feedrate correction module

After obtaining the set of local minimum feedrates, it is normally a basic requirement to move the cutter from the current extremal position to the next one without violating the contour error and drive constraints. However, in some extreme situations where the feedrate limits of two adjacent extremal regions are significantly different, the machine tool might be

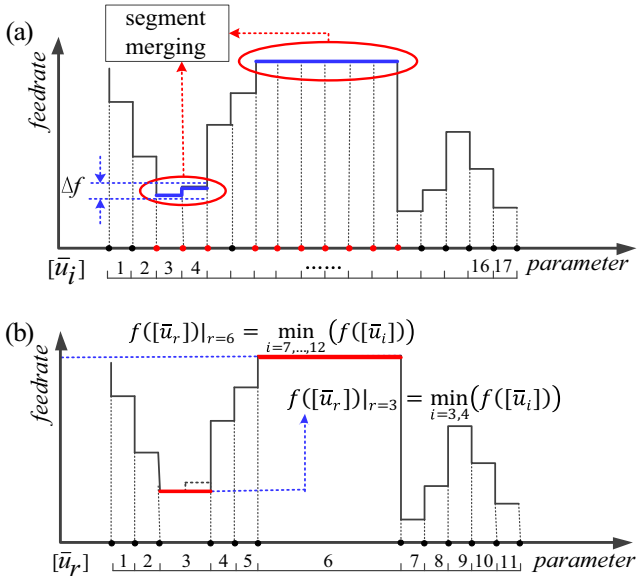

Fig. 5 The fusion of parameter intervals. (a) Original parameter intervals. (b) Parameter intervals after merging

incapable of accelerating or decelerating from the current local minimum to the next one without violating the prescribed constraints. Actually, it indicates that some of local minimum feedrates should be further adjusted to guarantee that the related constraints are satisfied when the most conservative feedrate profile constructed by the set of local minimum feedrates is given. As shown in Fig. 6, a bidirectional scanning operation is utilized here to adjust the local minimum feedrate values. In the parameter regions $[\overline{u}_4]$, $[\overline{u}_8]$, and $[\overline{u}_{11}]$, their associated local minimum feedrates can be found from the set $f([\overline{u}_r])$. And the parameter region $\left[\overline{u}_5^-, \overline{u}_7^+\right]$ is naturally referred as the transition region. Before the scanning operation, a quantic Bézier curve is introduced to express the local feedrate curve segment at the transition region $\left[\overline{u}_5^-, \overline{u}_7^+\right]$ under the most conservative situation, which is given as

$$f(t) = \sum_{i=0}^{n} b_i B_{i,n}(t) \quad 0 \le t \le 1 \tag{26}$$

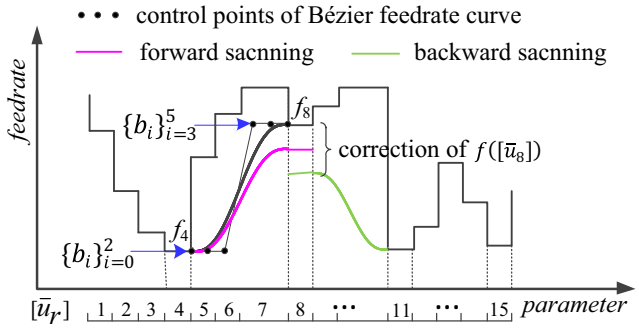

Fig. 6 The correction of local minimum feedrates based on a bidirectional scanning algorithm

where $[b_i]_{i=0}^n$ represents the vector of control points of the Bézier feedrate profile, $n+1$ is the number of control points, and $B_{i,n}(t)$ is the Bernstein basis function with the following analytical expression

$$B_{i,n}(t) = \begin{cases} \binom{n}{i}(1-t)^{n-i}t^i, & i = 0, \cdots, n \\ 0, & \text{otherwise} \end{cases}$$

Considering u and t are two different parameters, the mapping relation between them is needed to be known in advance, which can be expressed as

$$\begin{cases} t = \dfrac{u - \overline{u}_5^-}{\Delta u} \\ \Delta u = \overline{u}_7^+ - \overline{u}_5^- \end{cases} \tag{27}$$

where $u \in \left[\overline{u}_5^-, \overline{u}_7^+\right]$. To guarantee the C^2 continuity at the junction between Bézier curve and lines, namely, $\dot{f}(0) = \dot{f}(1) = \ddot{f}(0) = \ddot{f}(1) = 0$, the control points $(b_i)_{i=0}^2$ need to be identical, as well as $(b_i)_{i=3}^5$. Accordingly, their reference values are expressed by

$$\begin{aligned} b_i = f(t_i) &= \begin{cases} f_4 & i = 0, 1, 2; \\ f_8 & i = 3, 4, 5; \end{cases} \\ N_{i,0}(u) &= \begin{cases} 1, & u_i < u < u_{i+1} \\ 0, & \text{otherwise} \end{cases} \\ N_{i,k}(u) &= \frac{u - u_i}{u_{i+k} - u_i} N_{i,k-1}(u) + \frac{u_{i+k+1} - u}{u_{i+k+1} - u_{i+1}} N_{i+1,k-1}(u) \end{aligned} \tag{28}$$

Figure 6 shows the bidirectional scanning process, where the black solid line denotes the initial Bézier feedrate curve, the purple solid line represents the one after forward scanning, and the green solid line represents the one after backward scanning. In the forward scanning, if one or some of the prescribed constraints are out of their limits at the transition zones $\left[\overline{u}_5^-, \overline{u}_7^+\right]$ while the adjacent local minimum feedrate limits satisfy the condition $f_4 < f_8$, the relatively higher local minimum feedrate value f_8 is decreased with a regular increment $\Delta f = \alpha(f_8 - f_4)(0 < \alpha < 1)$ iteratively until the final desired feedrate value of f_8 is achieved without violating constraints. At the worst, the feedrate value f_8 will decrease to f_4, and hence the Bézier feedrate curve becomes a straight line. On this condition, it is certain that the constraints can be satisfied according to Eq. (23). The backward scanning operation is similar to that of forward scanning operation, and its related process will not be detailed here.

4.3 The proposed feedrate relaxation method

As shown in Fig. 7, when the process of feedrate limit correction is finished, the local minimum feedrate segments will be permanent. Considering that all the featured feedrate segments with local minimum and maximum feedrate values are exact without any constraint violations, we can make full use of such information to construct the feedrate profile in B-spline form with an exact configuration of knot sequence. On this basis, a feedrate relaxation algorithm is performed to prevent the prescribed constraints beyond their limits at the transition regions, in which the feedrate accelerates/decelerates from an extremal position to the next one. Equation (30) gives the explicit B-spline expression of the feedrate profile.

$$f(u) = \sum_{i=0}^{n} d_i N_{i,k}(u) \quad 0 \le u \le 1 \tag{30}$$

where $(d_i)_{i=0}^{n}$ represents the vector of control points of the B-spline feedrate profile, and $n+1$ is the number of control points. $\boldsymbol{U} = [u_0, \ldots, u_{n+k+1}]$ represents the knot sequence, k is the degree of B-spline curve and, $N_{i,k}(u)$ is the B-spline basis function with the recursive formulas as

4.3.1 Configuration of knot sequence of initial B-spline feedrate profile

Based on the local minimum and maximum feedrate limit segments, the exact configuration of knot sequence of the initial B-spline feedrate profile can be immediately realized. For a given set of feedrate limits and their associated parameter positions, three different cases may be encountered during the process of the configuration of knot sequence.

Case 1 Given a local maximum feedrate segment $[f_r]$, if its corresponding parameter range $[\overline{u}_r]$ satisfies $\left\lceil \left(\overline{u}_r^{+} - \overline{u}_r^{-}\right) / \Delta u \right\rceil = 1$, where $\lceil \cdot \rceil$ stands for the operation of taking a proximal integer, it usually means that a peak will appear at this parameter position of the feedrate profile. Accordingly, as shown in Fig. 8, three control points $(d_i)_{i=c}^{c+2}$ are set to f_r so as to generate

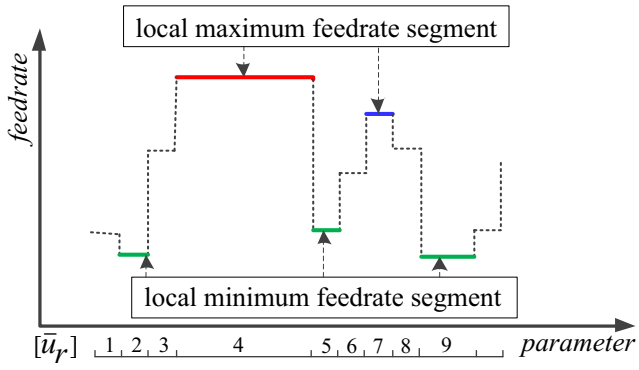

Fig. 7 The feedrate sequence after bidirectional scanning correction

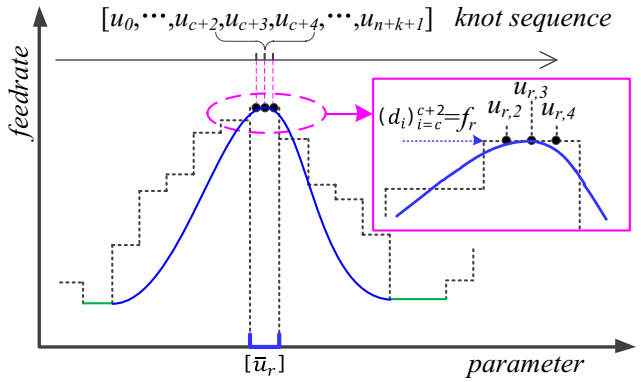

Fig. 8 The single-peak feedrate curve generation

a single-peak feedrate curve at the transition regions. And the corresponding knot spans $(u_i)_{i=c+2}^{c+4}$ which dominate the peak location of feedrate curve are given as $(u_{r,2}, u_{r,3}, u_{r,4})$. For this situation, the parameter interval $[\overline{u}_r]$ is first refined into four parts, and $u_{r,l}\,(l = 1, \ldots 5)$ denotes the concrete parameter, where $u_{r,1} = \overline{u}_r^{-}$, $u_{r,5} = \overline{u}_r^{+}$.

Case 2 Similarly, for a given local maximum feedrate segment $[f_r]$, if its corresponding parameter range $[\overline{u}_r]$ satisfies the condition $\left\lceil \left(\overline{u}_r^{+} - \overline{u}_r^{-}\right) / \Delta u \right\rceil \ge 2$, it means that the feed will maintain a constant speed within a wide parameter range. As a result, four control points are required to be set $(d_i)_{i=c}^{c+3} = f_r$, as shown in Fig. 9. Here, the related parameter segment $[\overline{u}_r]$ is refined into $(N_r - 1)$ parts in advance, and its corresponding parameter position is denoted as $u_{r,l}\ (l = 1, \ldots, N_r)$ and $u_{r,1} = \overline{u}_r^{-}$, $u_{r,N_r} = \overline{u}_r^{+}$. Specifically, the values and locations of knot spans $(u_i)_{i=c+2}^{c+5}$ can be determined as $(u_{r,2}, u_{r,3}, u_{r,N_r-2}, u_{r,N_r-1})$. By means of such a configuration of control points, the feed movement with constant speed can be achieved within the parameter range $(u_{r,3}, u_{r,N_r-2})$.

Case 3 As shown in Fig. 10, for any given local minimum feedrate segment $[f_r]$, four control points $(d_i)_{i=c}^{c+3}$ are configurated as f_r since a stable feed movement is preferred at the corner point of the tool path to improve machine

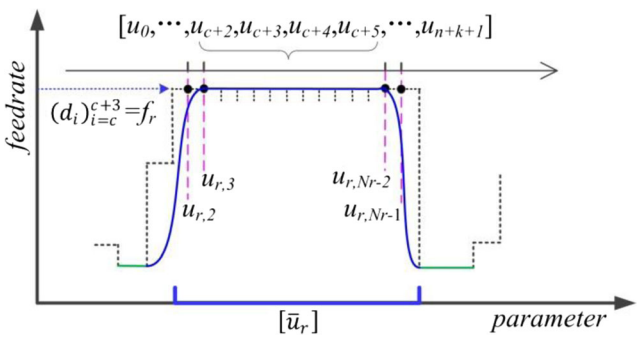

Fig. 9 The maximum constant feedrate curve generation

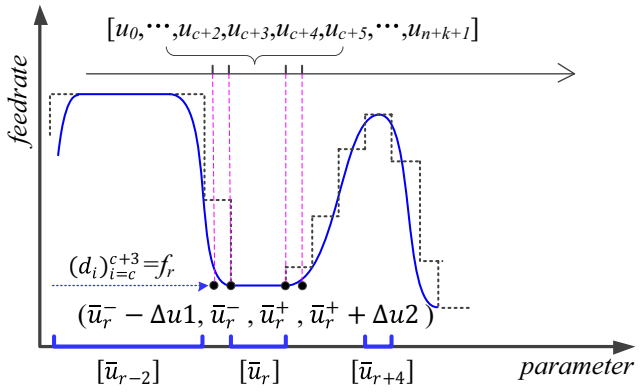

Fig. 10 The local minimum constant feedrate curve generation

performance. And the corresponding knot spans $(u_i)_{i=c+2}^{c+5}$ can be given as $(\bar{u}_r^- - \Delta u1,\ \bar{u}_r^-,\ \bar{u}_r^+,\ \bar{u}_r^+ + \Delta u2)$, where

$$\begin{cases} \Delta u1 = \left(\overset{+}{\bar{u}}_{r-2} - \overset{-}{\bar{u}}_{r-2}\right)/N_{r-2} \\ \Delta u2 = \left(\overset{+}{\bar{u}}_{r+4} - \overset{-}{\bar{u}}_{r+4}\right)/4 \end{cases}$$

From the above configuration of knot spans $(u_i)_{i=c+2}^{c+5}$ in Fig. 9, it is worth noting that the parameter positions $u_{r,\,l}$ of the first and last knot spans are set as $l=2$ and $l=N_r-1$, respectively. As shown in Fig. 11, a basic requirement is that the right boundary of segment $\bar{u}_d^+$ may at most reach the left boundary of segment $\bar{u}_{d+1}^-$, namely $\bar{u}_d^+ = \bar{u}_{d+1}^-$, and this will lead to the occurrence of interior knots with multiplicity 2 in the knot sequence $\boldsymbol{U}$. It is also allowed in the construction of B-spline feedrate profile.

Here, an adaptive knot sequence determination method is adopted to assign the knot sequence with the expression as

$$\boldsymbol{U} = [0,0,0,0,u_4,\cdots,u_k,\cdots,u_n,1,1,1,1]$$

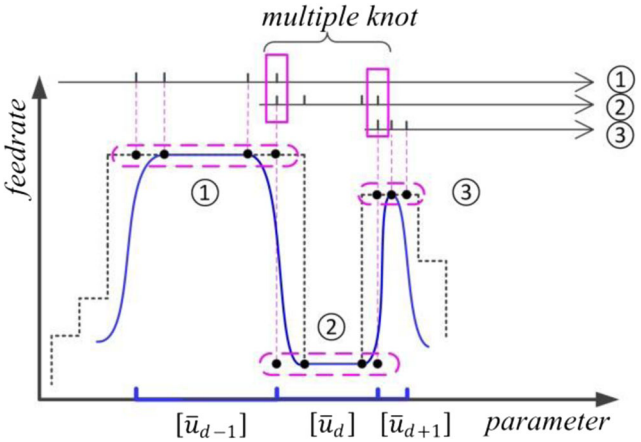

Fig. 11 An extreme situation of configuration of control points

where u_k represents the corresponding parametric position of knot of feedrate curve, and $n+5$ is the total number of the configured knot sequence. Finally, utilizing the proposed exact configuration method of knot sequence, one can rapidly construct an initial B-spline feedrate profile from the set of local feedrate limits.

4.3.2 Moving knot sequence-based feedrate relaxation

For the constructed initial feedrate curve represented in B-spline form, although the constraints have been fulfilled at the constant feedrate segments, constraint violations might occur at the transition regions, where the feedrate is in the accelerating or decelerating process. Hence, a feedrate relaxation algorithm is used to confine the constraints of transition regions based on a moving knot sequence strategy. During adjusting the knot sequence of B-spline feedrate curve, a basic principle of the knot spans at local minimum regions remains unchanged and only adjusting related knot spans at local maximum regions. That is, the movement of knot spans will only happen in the situation of case 1 and case 2.

For the situation of case 1, the general principle is only adjusting the values of control points while their knot spans remains unchanged. To make a detailed description of such adjusting procedure, assume $[\bar{u}_r]$ represents the current local maximum parameter segment, and its adjacent local minimum parameter segments are denoted by $[\bar{u}_p]$ and $[\bar{u}_q]$. Accordingly, the feedrate limits in these parameter segments are respectively indicated by f_r, f_p, and f_q. After configuration of the control points, the initial value of $(d_i)_{i=c}^{c+2}$ at the local maximum region is set as f_r, namely $(d_i)_{i=c}^{c+2} = f_r$. Let $f_m = \min(f_p, f_q)$, and the adjustable range of the values of $(d_i)_{i=c}^{c+2}$ can be specified as $[f_m, f_r]$. On this basis, if there exists constraint violation at the transition region $[\bar{u}_p^+,\ \bar{u}_q^-]$, the detailed adjustment of control points $(d_i)_{i=c}^{c+2}$ is carried out according to the following rules.

Rule 1 If the updated value $d_c \in (f_m, f_r]$ while $|d_c - f_m| > \delta$

only change the values of $(d_i)_{i=c}^{c+2}$ equally without changing their correspond knot spans $(u_i)_{i=c+2}^{c+4}$

else if $|d_c - f_m| \le \delta$

only the middle knot $(u_i)_{c+3}$ and control point $(d_i)_{c+1}$ remain, and delete the other two knots $(u_i)_{i=c+2,\ c+4}$ and the control points $(d_i)_{i=c,\ c+2}$

else

delete all the three knots $(u_i)_{i=c+2}^{c+4}$ and control points $(d_i)_{i=c}^{c+2}$

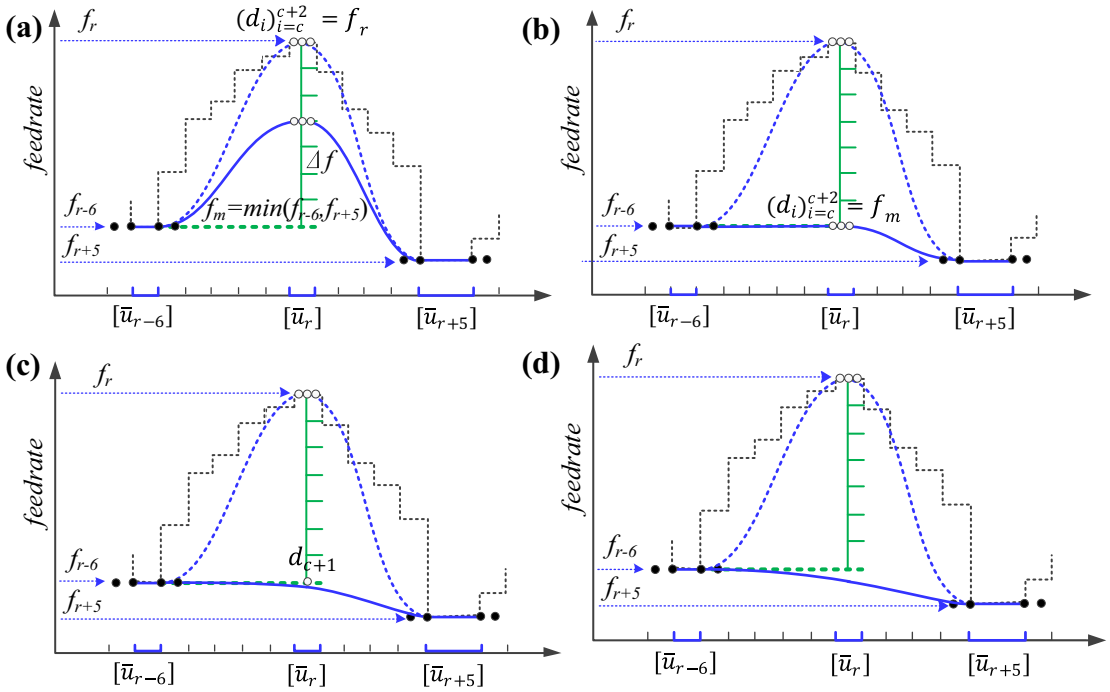

Fig. 12 The adjustment of feedrate curve for case 1. (a) Three control points synchronously decrease by increment Δf. (b) The lowest position the three control points could reach to. (c) After deleting the control points of both sides. (d) After deleting the last control point

where δ is a small quantity. To realize a fast adjustment of $(d_i)_{i=c}^{c+2}$, the total range of $(f_m, f_r]$ can be divided into several subintervals at first with an acceptable step length. Then, control points $(d_i)_{i=c}^{c+2}$ are placed and constraint evaluation is performed at these special positions, from which the feasible value of $(d_i)_{i=c}^{c+2}$ can be determined. Generally, it is enough for the feedrate scheduling in this manner, although a dichotomy algorithm can be used for finding more precise control points $(d_i)_{i=c}^{c+2}$. For example, as shown in Fig. 12(a), three control points $(d_i)_{i=c}^{c+2}$ are configured at the local maximum regions $[\overline{u}_r]$, and its adjacent local minimum regions are represented as $[\overline{u}_{r-6}]$ and $[\overline{u}_{r+5}]$, respectively. If there exist constraint violations at the transition regions $[\overline{u}_{r-6}^{+}, \overline{u}_{r+5}^{-}]$, the values of control points $(d_i)_{i=c}^{c+2}$ will be reduced recursively with a given value Δf sequentially

$$\begin{cases} \Delta f = (f_r - f_m)/G; \\ f_m = \min(f_{r-6}, f_{r+5}); \end{cases}$$

where G represents the refined number of the specified range $(f_m, f_r]$. If $(d_i)_{i=c}^{c+2}$ decreased to a value close to f_m while the constraints still remain beyond their limits, as shown in Fig. 12(b), one can delete d_c and d_{c+2} from the local maximum regions, as well as knots $(u_i)_{i=c+2,\ c+4}$,

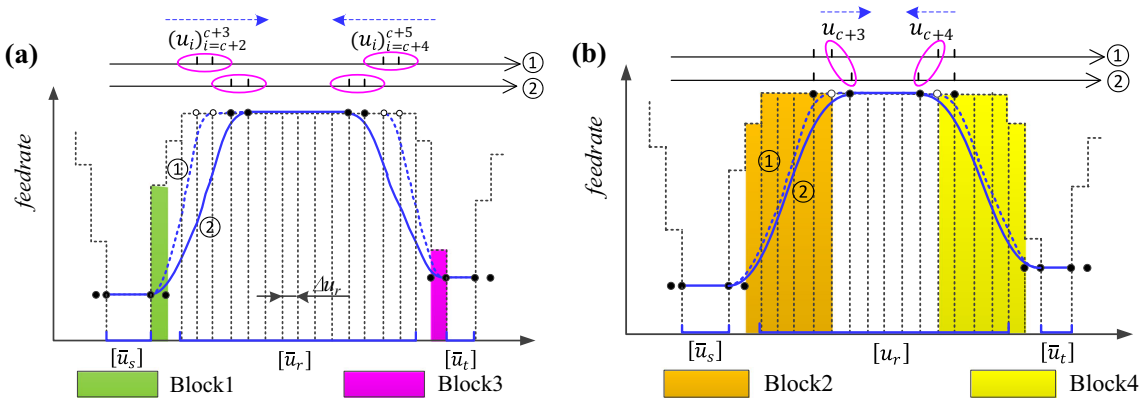

Fig. 13 The adjustment of feedrate curve for case 2. (a) Control points adjustment when constraints violate in Block B_1 and B_3. (b) Control point adjustment when constraints violate in Block B_2 and B_4

thus slowing down the accelerating or decelerating process as shown in Fig. 12(c), which is benefitial of reducing the excessive constraints. In the extreme case, as shown in Fig. 12(d), the last control point d_{c+1} and knot u_{c+3} are also deleted from $[\overline{u}_r]$. That is, there is no need to configurate control points at this local maximum region since the feedrate profile has approached the base curve of feedrate obtained from all local minimum feedrates. Based on the conditions of section 4.2, the prescribed constraints must be fulfilled in this situation. For the situation of case 2, the fundamental principle is only adjusting the knot spans, while their control point values remain unchanged. During the adjusting process, if any two of the knots encounter each other, one of the encountered knots needs to be deleted, and in this situation case 2 will be converted into case 1. Assume that the current local maximum parameter segment is $[\overline{u}_r]$, and its adjacent local minimum parameter segments are, respectively, $[\overline{u}_s]$ and $[\overline{u}_t]$. For achieving an exact adjustment of knot spans, the corresponding transition region is divided into four blocks $[\overline{u}_s^+, \overline{u}_s^+ + \Delta u_r]$, $[\overline{u}_s^+ + \Delta u_r, u_{r,3}]$, $[u_{r,N_r}, \overline{u}_t^- - \Delta u_r]$, and $[\overline{u}_t^- - \Delta u_r, \overline{u}_t^-]$, which are denoted as

B_1, B_2, B_3, and B_4, respectively. After configuration of the four knots $(u_i)_{i=c+2}^{c+5}$ at the local maximum region $[\overline{u}_r]$, different operations are necessarily determined for each block. And the corresponding moving rules of knot sequence are presented as follows.

Rule 2_a If constraint violation occurs at Block B_1 (B_3)

both knots $(u_i)_{i=c+2}^{c+3}$ ($(u_i)_{i=c+4}^{c+5}$) are equivalently moved toward the right (left) with a specified parameter interval until without constraint violations.

Rule 2_b If constraint violation occurs at Block B_2 (B_4)

only move knot u_{c+3} (u_{c+4}) toward the right (left) until without violated constraints.

In detail, as shown in Fig. 13, four knots $(u_i)_{i=c+2}^{c+5}$ are configurated at the local maximum regions $[\overline{u}_r]$. During the adjusting process, if there exist constraint violations in block B_1, the feedrate curve can be locally deformed by moving $(u_i)_{i=c+2}^{c+3}$ toward the right synchronously with a predefined parameter increment Δu_r, thus slowing down the accelerating or decelerating process until the constraints in block B_1 are all fulfilled. Then, those contents in block B_2 are evaluated using the same way. Theoretically, the corresponding feedrate curve in block B_2 can be also adjusted by synchronously moving knots $(u_i)_{i=c+2}^{c+3}$ to the right. Here, in order to simplify the operation, the knot u_{c+2} is normally fixed and only moves u_{c+3} toward the right for the feedrate relaxation.

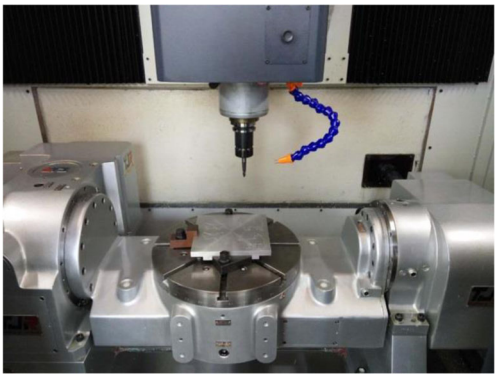

Fig. 14 Multi-axis CNC machine tool used in experiment

Since the feedrate curve adjustment of $B_3(B_4)$ is similar to that of $B_1(B_2)$, therefore, the corresponding moving process of $(u_i)_{i=c+4}^{c+5}$ will not be stated here. Besides, an extreme situation is worth noting that the knots u_{c+3} and u_{c+4} may encounter each other during the process of adjustment of knot sequence. In this situation, one can delete one of them to maintain three knots along the parameter segment $[\overline{u}_r]$, and simultaneously delete one of the control points $(d_i)_{i=c}^{c+3}$; thus, the situation of adjustment of control points is converted into case 1 as illustrated in Fig. 12. Finally, a smooth feedrate profile can be obtained with entirely limited contour error and axis jerks through several rounds of adjustment.

5 Results and discussions

In order to verify the proposed method, several physical cutting experiments are conducted on AL Alloy 6061 plate with an 8-mm-diameter ball-end carbide cutter. The depth of cut is 0.05 mm in the finished operation and the spindle speed is set as 4000 rpm. The cutting experimental setup is an open architecture CNC system equipped with Yaskawa AC servo motor and CACR_JUM25D2A driver, as shown in Fig. 14. The corresponding interpolation period of CNC system is set as 4 ms. The ball screw lead in the feed system is 10 mm/pitch,

Table 2 Constraints in feedrate scheduling for experiment 1

Constraints	Experiment setting (x/y)		
	Test_1_1	Test_1_2	Unit
Axis velocity	30/30	30/30	mm/s
Axis acceleration	400/300	400/300	mm/s^2
Axis jerk	–	6000/6000	mm/s^3

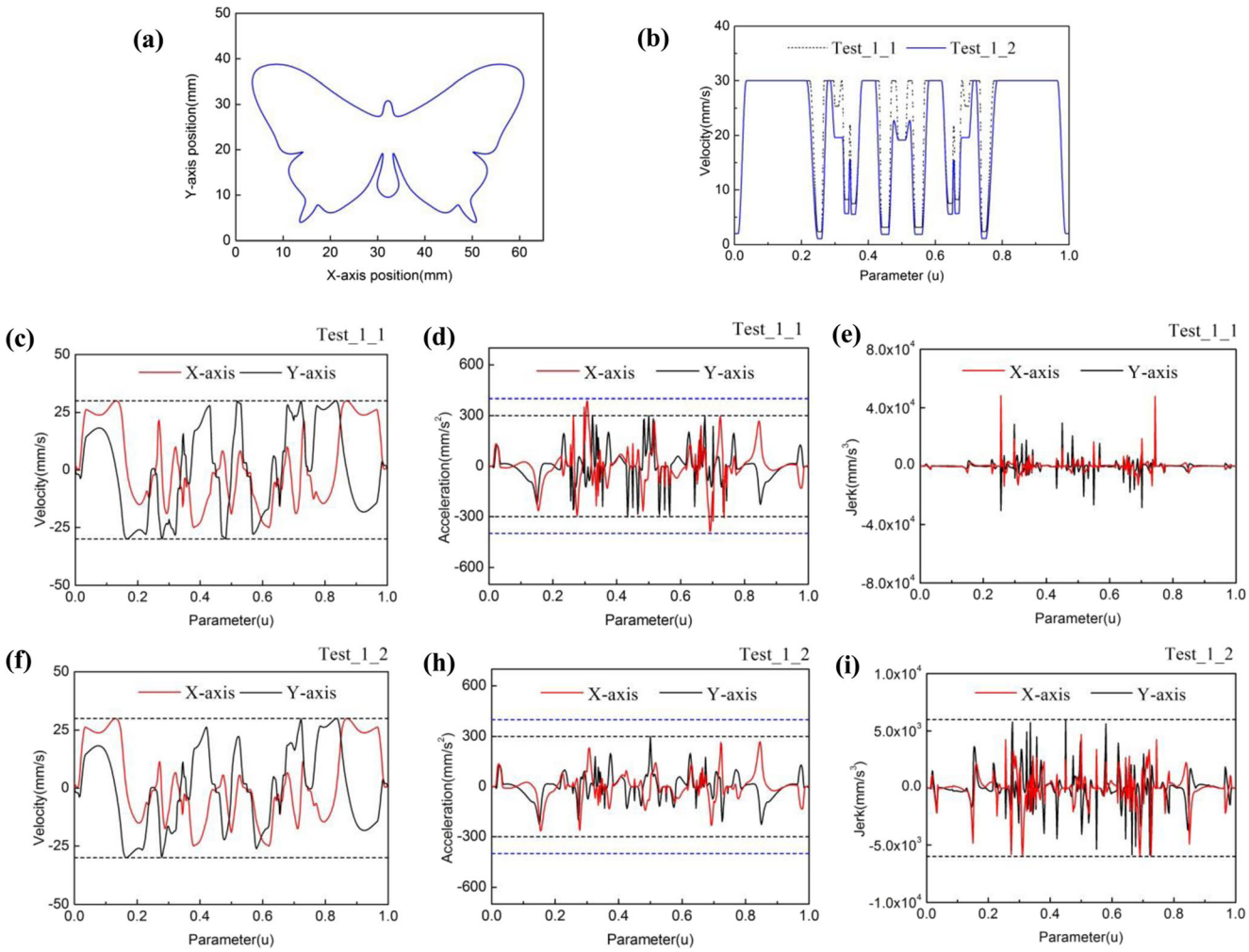

Fig. 15 Comparison of feedrate scheduling results between Test_1_1 and Test_1_2. (a) Tool path. (b) Feedrate curves. (c) Axis velocities of Test_1_1. (d) Axis accelerations of Test_1_1. (e) Axis jerks of Test_1_1. (f) Axis velocities of Test_1_2. (h) Axis accelerations of Test_1_2. (i) Axis jerks of Test_1_2

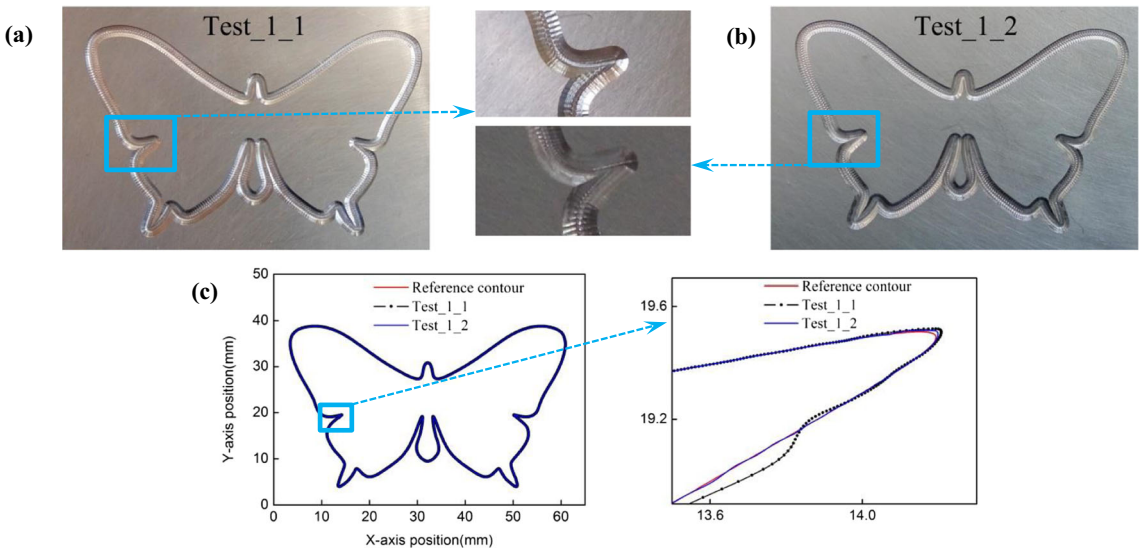

Fig. 16 Experimental results. (a) Physical cutting result of Test_1_1. (b) Physical cutting result of Test_1_2. (c) Trajectory following results and its details

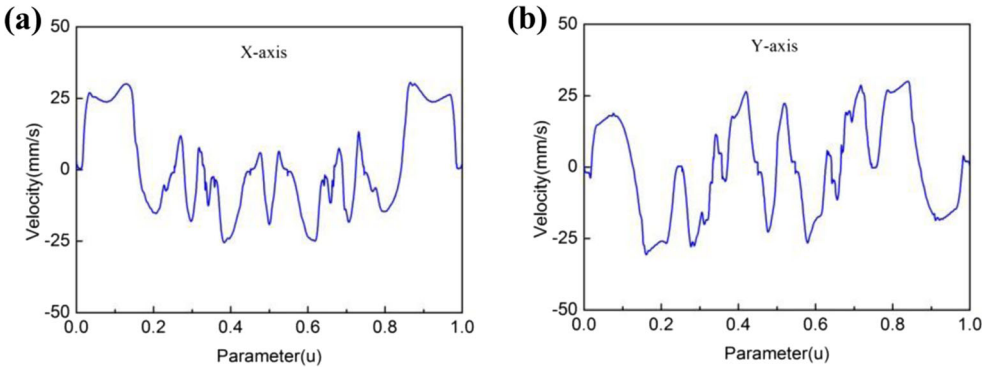

Fig. 17 The actual velocity curves for Test_1_2. (a) x-axis velocity. (b) y-axis velocity

and the position feedback signal can be obtained directly from the optical linear scales with 500 × 256 pulses per revolution. In addition, the related coefficient $K_e = 36.900$ for the drive axis is identified according to Xi et al. [59]. In the real operation, the feedrate for a given parametric tool path usually needs to accelerate from a specified value at the start of the tool path, and decreases to a specified value at the end of the tool path. Here, both of the start and end feedrate values are set as 2 mm/s to avoid the abrupt change of acceleration at the beginning and ending, and the maximum allowable feedrate is specified as 30 mm/s.

5.1 Experiment 1: Verification of drive constraints

5.1.1 Experimental results

To illustrate the effectiveness of the proposed feedrate scheduling method on confining the drive constraints, two sets of experiments with separate constraints of acceleration and jerk are conducted, in which the axis jerk constraint is only considered in Test_1_2 for a comparison purpose. And the detailed parameters used in the feedrate scheduling are given in Table 2. Figure 15(a) shows the desired path contour expressed by the NURBS curve with 51 control points. From this figure, it can be seen that there exist multiple high-curvature regions along the path curve, in which the prescribed constraints are extremely possible to exceed their predefined limitations. During the feedrate scheduling, the parameter domain of the tool path is discretized into 100 uniform intervals, and for each parameter interval, the feedrate limit is obtained by using the proposed decoupled scheme. Afterwards, the local minimum feedrate values are updated in the feedrate correction module by using a bidirectional scanning algorithm with a proportional coefficient $\alpha = 0.2$. Meanwhile, a parameter merging operation is also performed on adjacent parameter segments if their feedrate limits

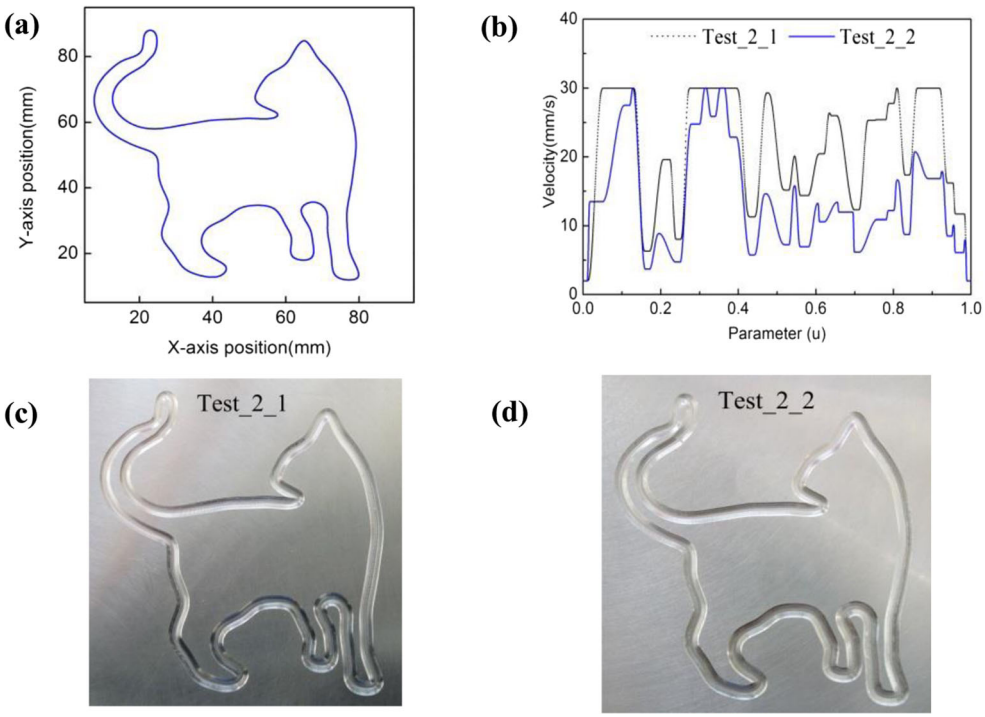

Fig. 18 Experimental results. (a) Tool path. (b) Feedrate curves. (c) Physical cutting result of Test_2_1. (d) Physical cutting result of Test_2_2

Table 3 Constraints in feedrate scheduling for experiment 2

Constraints	Experiment setting (x/y)		
	Test_2_1	Test_2_2	Unit
Axis velocity	30/30	30/30	mm/s
Axis acceleration	150/100	150/100	mm/s^2
Axis jerk	1500/1000	1500/1000	mm/s^3
Contour error	–	0.01	mm

fluctuate within the range of [−0.2 mm/s, 0.2 mm/s]. Then, using the proposed moving knot sequence-based feedrate relation algorithm, one can obtain the final planned feedrate curves with the above-prescribed constraints as shown in Fig. 15(b), which are respectively denoted by the dark and blue-colored lines. And their associated kinematical character in terms of velocity, acceleration, and jerk of the feed drives is also presented in Fig. 15(c)–(i). Using the generated feedrate profiles plotted in Fig. 15(b), the cutting experimental results are obtained and shown in Fig. 16. Figure 17 illustrates the actual velocities of x- and y-axes for the case of jerk-limited processing.

5.1.2 Discussion for experiment 1

As shown in Fig. 15(b), the generated feedrate profile by using the proposed method maintains a good smoothness characteristic along the entire tool path, which is the benefit of suppressing unwanted feedrate fluctuation and achieving a stable cutting process. From Fig. 15(c)–(i), it can be seen that the x-axis accelerations of Test_1_1 and Test_1_2 are both confined within the allowable range [− 400 mm/s^2, 400 mm/s^2], and the y-axis accelerations for both of cases are also limited within [− 300 mm/s^2, 300 mm/s^2]. Besides, from Fig. 15(i), we can see that the x- and y-axis jerks of Test_1_2 are totally bounded by the preset range of [− 6000 mm/s^3, 6000 mm/s^3]. In contrast to that of Test_1_1, the high-frequency jerk components are significantly reduced, which is favorable to a smoother cutter movement. Further, in Fig. 17, it is clear that the nominal and actual axis velocities have good agreement both in the shape and magnitude, thus indicating the effectiveness of the proposed feedrate scheduling method on confining drive constraints. In addition, from the physical cutting results as illustrated in Fig. 16, the axis jerk-limited feedrate profile exhibits a more satisfactory performance on ensuring the surface texture quality as compared with the axis acceleration-limited situations, and the vibration phenomena are significantly alleviated at the tight curvature zones.

5.2 Experiment 2: Verification of contour error

5.2.1 Experimental results

As shown in Fig. 18(a), a cat-shaped path contour is employed for the second cutting experimental verification. It is obvious to note that the path curvature varies dramatically around the sharp corner, and the contouring error probably exceeds its maximum allowable value if an improper feedrate is given at these sensitive regions. To validate the derived relationship between the contour error and feedrate, physical cutting experiment with limited contour error is conducted on the cat-shaped path curve. Considering that undesired chatter of cutter induced by the excessive acceleration and jerk might influence the contouring accuracy, the kinematical performance of the servo drives is considered as an additional constraint along with the contour error limitation in the feedrate scheduling. For achieving reliable model verification, a comparison is conducted between two cases of single-drive constraint and compound constraints of both contour error and drive constraint. The detailed process constraints are presented in Table 3. Figure 18(b) shows the generated feedrate curves by using the proposed method, from which it can be seen that the nominal feedrate gradually decreases to a lower value when approaching the sharp corner area. Afterwards, utilizing these scheduled feedrate profiles, the final machined parts are obtained as it is demonstrated in Fig. 18(c)–(d). Figure 19(a)

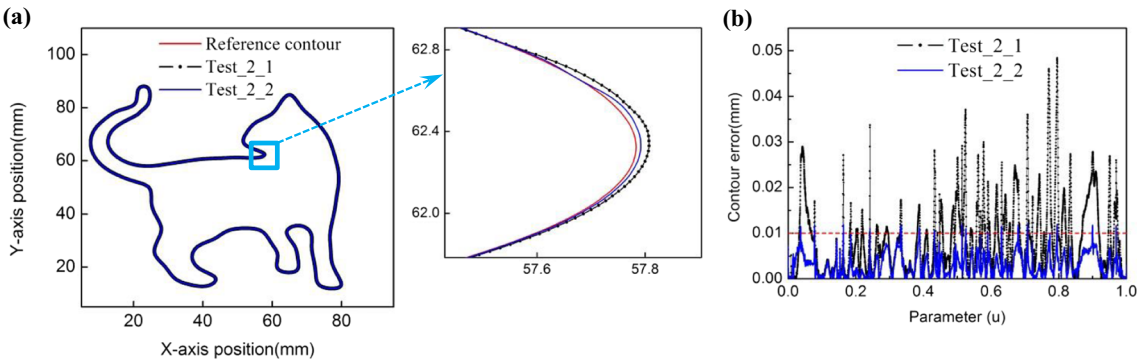

Fig. 19 Comparison of contouring performance between Test_2_1 and Test_2_2. (a) Trajectory following results and its details. (b) Contour errors for the cat curve

Table 4 Constraints in feedrate scheduling for experiment 2

Contour error (mm)	Experiment setting	
	Test_2_1	Test_2_2
Maximum value	0.0484	0.0119
Mean value	0.0087	0.0030

shows the actual motion position measured from the optical linear scales, and the actual contour errors are also computed based on these collected experimental data, which are plotted in Fig. 19(b). To make a clear observation of the contouring performance by using the proposed feedrate scheduling method, the associated statistical experimental data are also summarized in Table 4.

5.2.2 Discussion for experiment 2

From the cutting experimental results in Fig. 18(c)–(d), both Test_2_1 and Test_2_2 maintain a good surface quality of the cutting trajectory. To some extent, this further exhibits the capability of the proposed method on improving the smoothness of the feeding motion. According to the comparative plots of measured tool paths and reference trajectory in Fig. 19(a), we can also find that the actual path contour of Test_2_2 is closer to the reference one than that of Test_2_1. And the dynamic contour error of Test_2_2 is also generally limited to the required accuracy level, as it is given in Fig. 19(b). In addition, from the experimental data summarized in Table 4, the maximum contouring errors of Test_2_2 is 0.0119 mm, and the average contour error is also totally confined within its predefined range. Although there is a slight overrun at some sensitive regions, the experimental result is still acceptable for the model verification, since the contouring performance of machine tool is combinedly affected by many factors involving the tracing accuracy of the servo system, the resolution of encoder used in feedback measurement devices, as well as the motion synchronization of drive axes, etc.

In summary, according to above experimental results, it is reasonable to figure out that the feedrate scheduling method presented here has the ability of accurate control of contour error and axis jerk. And the smoothness of cutter movement can be simultaneously enhanced by using the proposed method.

6 Conclusions

In this paper, an adaptive feedrate scheduling method with confined contour error and axis jerk constraint is investigated for free-form contour machining. Different from the previous works, our method is based on a moving knot sequence strategy, and the process-related constraints such as the axis acceleration, axis jerk, and contour error can be systematically considered into the feedrate scheduling model. As an important characteristic, the issue of multi-constraint feedrate scheduling is nicely reduced to the construction of finite curve segments via an explicit B-spline expression of the feedrate profile, and the advantages of the proposed method lie in its easier implementation and direct control ability of constraints. Therefore, one can obtain the final desired feedrate profile without excessive computation complexity. Besides, the proposed method has also strong compatibility to add or relax more kinematical constraints into the feedrate scheduling model.

In order to evaluate the proposed method, several typical experimental tests are conducted. According to the experimental results, it is proved that the proposed method is robust and effective to limit the prescribed constraints. By adding the axis jerk constraints in the feedrate scheduling, the cutting performance of machine tool is also improved as compared with that of the acceleration limited situation. And it is able to obtain a better machining quality if the constraint of cutting force is also considered. However, all these need further research.

Acknowledgments This research is supported by the NSFC (51525501), SCP (TZ2016006-0102), and STBD (2016RD08).

References

1. Wang Y, Yang D, Liu Y (2014) A real-time look-ahead interpolation algorithm based on Akima curve fitting. Int J Mach Tools Manuf 85:122–130
2. Yeh SS, Hsu PL (2002) Adaptive-feedrate interpolation for parametric curves with a confined chord error. Comput Aided Des 34: 229–237
3. Cheng CW, Tai MC (2004) Real-time variable feed rate NURBS curve interpolator for CNC machining. Int J Adv Manuf Technol 23:865–873
4. Yong T, Narayanaswami R (2003) A parametric interpolator with confined chord errors, acceleration and deceleration for NC machining. Comput Aided Des 35:1249–1259
5. Nam SH, Yang MY (2004) A study on a generalized parametric interpolator with real-time jerk-limited acceleration. Comput Aided Des 36:27–36
6. Zhao H, Zhu L, Ding H (2013) A parametric interpolator with minimal feed fluctuation for CNC machine tools using arc-length compensation and feedback correction. Int J Mach Tools Manuf 75: 1–8
7. Liu X, Ahmad F, Yamazaki K, Mori M (2005) Adaptive interpolation scheme for NURBS curves with the integration of machining dynamics. Int J Mach Tools Manuf 45:433–444
8. Lai JY, Lin KY, Tseng SJ, Ueng WD (2008) On the development of a parametric interpolator with confined chord error, feedrate, acceleration and jerk. Int J Adv Manuf Technol 37:104–121

9. Xu RZ, Xie L, Li CX, Du DS (2008) Adaptive parametric interpolation scheme with limited acceleration and jerk values for NC machining. Int J Adv Manuf Technol 36(3–4):343–354
10. Ni H, Yuan J, Ji S, Zhang C, Hu T (2018) Feedrate scheduling of NURBS interpolation based on a novel jerk-continuous ACC/DEC algorithm. IEEE Access
11. Liu HD, Xi XC, Liang W, Chen M, Chen H, Zhao WS (2018) A look-ahead transition algorithm for jump motions with short line segments in EDM. Int J Adv Manuf Technol 95:1409–1419
12. Jin Y, He Y, Fu J, Lin Z, Gan W (2014) A fine-interpolation-based parametric interpolation method with a novel real-time look-ahead algorithm. Comput Aided Des 55:37–48
13. Luo FY, Zhou YF, Yin J (2007) A universal velocity profile generation approach for high-speed machining of small line segments with look-ahead. Int J Adv Manuf Technol 35:505–518
14. Huang J, Zhu LM (2016) Feedrate scheduling for interpolation of parametric tool path using the sine series representation of jerk profile. Proc Inst Mech Eng B J Eng Manuf 231(13):2359–2371
15. Wang Y, Yang D, Gai R, Wang S, Sun S (2015) Design of trigonometric velocity scheduling algorithm based on pre-interpolation and look-ahead interpolation. Int J Mach Tools Manuf 96:94–105
16. Ye Z, Han P, Yang S (2014) SOPC based optimized feedrate scheduling for NURBS interpolation. In: Proceedings of 2014 I.E. International Conference on Mechatronics and Automation, pp 269–274
17. Liu X, Peng J, Si L, Wang Z (2016) A novel approach for NURBS interpolation through the integration of accjerk-continuous-based control method and look-ahead algorithm. Int J Adv Manuf Technol 88:961–969
18. Du X, Huang J, Zhu LM (2015) A complete S-shape feed rate scheduling approach for NURBS interpolator. J Comput Des Eng 2:206–217
19. Liu M, Huang Y, Yin L, Guo J, Shao X, Zhang G (2014) Development and implementation of a NURBS interpolator with smooth feedrate scheduling for CNC machine tools. Int J Mach Tool Manu 87:1–15
20. Zhao H, Zhu L, Ding H (2013) A real-time look-ahead interpolation methodology with curvature-continuous B-spline transition scheme for CNC machining of short line segments. Int J Mach Tool Manu 65(2013):88–98
21. Jahanpour J, Alizadeh MR (2015) A novel acc-jerk-limited NURBS interpolation enhanced with an optimized S-shaped quintic feedrate scheduling scheme. Int J Adv Manuf Technol 77(9): 1889–1905
22. Wang X, Wang J, Rao Z (2010) An adaptive parametric interpolator for trajectory planning. Adv Eng Softw 41:180–187
23. Leng HB, Wu YJ, Pan XH (2008) Research on cubic polynomial acceleration and deceleration control model for high speed NC machining. J Zhejiang Univ Sci A 9(3):358–365
24. Fan W, Gao XS, Yan W, Yuan CM (2012) Interpolation of parametric CNC machining path under confined jounce. Int J Adv Manuf Technol 62(5–8):719–739
25. Jeon JW, Ha YY (2000) A generalized approach for the acceleration and deceleration of industrial robots and CNC machine tools. IEEE Trans Ind Electron 47(1):133–139
26. Bharathi A, Dong J (2016) Feedrate optimization for smooth minimum-time trajectory generation with higher order constraints. Int J Adv Manuf Technol 82:1029–1040
27. Liang F, Zhao J, Ji S (2017) An iterative feed rate scheduling method with confined high-order constraints in parametric interpolation. Int J Adv Manuf Technol 92:2001–2015
28. Zhang K, Yuan C-M, Gao X-S, Li H (2012) A greedy algorithm for feedrate planning of CNC machines along curved tool paths with confined jerk. Robot Comput Integr Manuf 28(4):472–483
29. Zhang K, Yuan CM, Gao XS (2013) Efficient algorithm for time-optimal feedrate planning and smoothing with confined chord error and acceleration. Int J Adv Manuf Technol 66:1685–1697
30. Erkorkmaz K, Chen Q-G, Zhao M-Y, Beudaert X, Gao X-S (2017) Linear programming and windowing based feedrate optimization for spline toolpaths. CIRP Ann Manuf Technol 66:393–396
31. Liu H, Liu Q, Sun P, Liu Q, Yuan S (2017) The optimal feedrate planning on five-axis parametric tool path with geometric and kinematic constraints for CNC machine tools. Int J Prod Res 55(13): 3715–3731
32. Beudaert X, Lavernhe S, Tournier C (2012) Feedrate interpolation with axis jerk constraints on 5-axis NURBS and G1 tool path. Int J Mach Tools Manuf 57:73–82
33. Sencer B, Altintas Y, Croft E (2008) Feed optimization for five-axis CNC machine tools with drive constraints. Int J Mach Tools Manuf 48:733–745
34. Mansour S, Seethaler R (2017) Feedrate optimization for computer numerically controlled machine tools using modeled and measured process constraints. ASME J Manuf Sci Eng 139(1):011012
35. Yang DCH, Kong T (1994) Parametric interpolator versus linear interpolator for precision CNC machining. Comput Aided Des 26(3):225–234
36. Yeh SS, Hsu PL (1999) The speed-controlled interpolator for machining parametric curves. Comput Aided Des 31:347–359
37. Chuang HY, Liu CH (1991) Cross-coupled adaptive feedrate control for multiaxis machine tools. J Dyn Syst Meas Control 113:451–457
38. Yeh SS, Hsu PL (2000) A new approach to bi-axial cross-coupled control, in: Proceedings of the 2000 IEEE International Conference on Control Applications, pp 168–173
39. Yeh SS, Hsu PL (2002) Estimation of the contouring error vector for the cross- coupled control design. IEEE/ASME Trans Mechatronics 7:44–51
40. Chen SL, Liu LH, Ting SC (2002) Contouring control of biaxial systems based on polar coordinates. IEEE/ASME Trans Mechatronics 7:329–345
41. Huo F, Xi XC, Poo AN (2012) Generalized Taylor series expansion for free-form two-dimensional contour error compensation. Int J Mach Tools Manuf 53:91–99
42. Sencer B, Altintas Y (2009) Modeling and control of contouring errors for five-axis machine tools—part I: modeling. J Manuf Sci Eng 131:1–8
43. Zhu L, Zhao H, Ding H (2013) Real-time contouring error estimation for multi-axis motion systems using the second-order approximation. Int J Mach Tools Manuf 68:75–80
44. Pi S, Liu Q, Liu Q (2018) A novel dynamic contour error estimation and control in high-speed CNC. Int J Adv Manuf Technol 96:547–560
45. Yang M, Yang J, Ding H (2018) A high accuracy on-line estimation algorithm of five-axis contouring errors based on three-point arc approximation. Int J Mach Tools Manuf 130–131:73–84
46. Yang J, Li Z (2011) A novel contour error estimation for position loop-based cross-coupled control. IEEE/ASME Trans Mechatronics 16:643–655
47. Zhang D, Yang J, Chen Y, Chen Y (2015) A two-layered cross coupling control scheme for a three-dimensional motion control system. Int J Mach Tools Manuf 98:12–20
48. Sencer B, Altintas Y (2009) Modeling and control of contouring errors for five-axis machine tools—part II: precision contour controller design. J Manuf Sci Eng Trans ASME 131:0310073
49. Barton KL, Alleyne AG (2008) A cross-coupled iterative learning control design for precision motion control. IEEE Trans Control Syst Technol 16(6):1218–1231
50. Lam D, Manzie C, Good MC (2013) Model predictive contouring control for biaxial systems. IEEE Trans Control Syst Technol 21: 552–559

51. Yang SY, Ghasemi AH, Lu XX, Okwudire CE (2015) Precompensation of servo contour errors using a model predictive control framework. Int J Mach Tools Manuf 98:50–60
52. Davis TA, Shin YC, Yao B (2014) Adaptive robust control of circular machining contour error using global task coordinate frame. J Manuf Sci Eng 137:014501
53. Bharathi A, Dong J (2015) Feedrate optimization and trajectory control for micro/nanopositioning systems with confined contouring accuracy. Proc Inst Mech Eng B J Eng Manuf 229(7): 1193–1205
54. Wang J, Sui Z, Tian YT, Wang XL, Fang L (2015) A speed optimization algorithm based on the contour error model of lag synchronization for CNC cam grinding. Int J Adv Manuf Technol 80: 1421–1432
55. Lin MT, Tsai MS, Yau HT (2007) Development of a dynamics-based NURBS interpolator with real-time look-ahead algorithm. Int J Mach Tools Manuf 47:2246–2262
56. Dong J, Wang T, Li B, Ding Y (2014) Smooth feedrate planning for continuous short line tool path with contour error constraint. Int J Mach Tools Manuf 76:1–12
57. Dong J, Stori JA (2007) Optimal feed-rate scheduling for high-speed contouring. J Manuf Sci Eng 129(1):63–76
58. Jia Z, Song D, Ma J, Hu G, Su W (2016) A NURBS interpolator with constant speed at feedrate-sensitive regions under drive and contour- error constraints. Int J Mach Tools Manuf 116:1–17
59. Xi XC, Poo AN, Hong GS (2009) Improving contouring accuracy by tuning gains for a bi-axial CNC machine. Int J Mach Tools Manuf 49:395–406